Scientific Research

Effect of Synthesis Routes on Microstructure of Nanocrystalline Cerium Oxide Powder

Ashutosh Sharma

Department of Metallurgical and Materials Engineering, Indian Institute of Technology Kharagpur, Kharagpur, India.
Email: stannum.ashu@gmail.com

ABSTRACT

The effect of different processing routes on the microstructure of nanocrystalline ceria powder has been investigated. The nanocrystalline ceria is produced by solid state high energy ball milling (HEBM) and liquid state solution combustion synthesis (SCS) method. The liquid state route consists of a high temperature combustion reaction to form ceria from an aqueous solution of cerium ammonium nitrate (CAN) as an oxidizer and citric acid (CA) plus glycine (G) as mixed fuels. The powders have been characterized using techniques of X-ray diffraction (XRD), particle size analysis, scanning electron microscopy (SEM), and transmission electron microscopy (TEM). The microstructural characterizations show that the particle size distribution of the ball milled ceria powder is much wider than that of ceria produced by the SCS. The scanning electron micrographs show that the ball milled ceria powders are compact and dense structure while SCS ceria powders are scattered and porous.

Keywords: Ball Milling; Solution Combustion; Ceria; Nanocrystalline

1. Introduction

Nanocrystalline ceria has been a supreme choice for advanced engineering applications such as, electronic, photonic, fuel cells, sensing device etc., and therefore it cannot be ignored by present researchers [1-4]. In literature, there are several routes through which a nanocrystalline ceria can be achieved, for instance, high energy ball milling, spray deposition, magnetron sputtering, solution combustion synthesis, pulse electro- deposition, sol-gel method, hydrothermal techniques, etc. [5-9]. From economical point of view, modern researchers are very keen to use high energy ball milling technique to produce nanocrystalline powders owing to its simple and environmental friendly nature while the other methods are more expensive. They require high temperature maintenance, inert atmosphere and/or hazardous chemicals [6-9]. However, the solution combustion synthesis method is very quick and easy to talk about and also consumes less time. It involves a high temperature combustion of aqueous solution of an oxidiser and a fuel. Such a high temperature reaction can vaporize low boiling point constituents resulting in highly pure products [10]. However, the process needs a great care due to the explosive nature of the reactions involved [11].

In the present work, the effects of HEBM and SCS routes on the microstructure of nanoceria powders are evaluated. HEBM has been performed for 20 hs to obtain nano-sized ceria particles from as-received ceria powders. SCS has been carried out by using (a) CAN and G + CA, where CAN is cerium ammonium nitrate, G is glycine and CA is citric acid. The produced ceria powders have been characterized and compared for their particle size, size distribution and microstructural evolution.

2. Experimental Procedure

### 2.1. Solid State Route—High Energy Ball Milling

High energy ball milling (HEBM) of as received ceria powders (Loba Chemie, 99.8%) is carried out using cemented tungsten carbide milling media with toluene as the process control agent. The mill (Fritsch Pulverissette-4, dual drive) is operated at a main disc speed (ω) 300 rpm and planet speed of (Ω) 540 rpm with a transmission ration (Ω/ω) of 1.8. The transmission ratio is the ratio of the man disc speed (Ω) to the speed of the planets (ω). According to (Ω/ω) the rotation speed choice, we can have the shock mode process (SMP) when $\Omega \gg \omega$, and the friction mode processes (FMP) when $\Omega \ll \omega$ [12]. For our case we selected the shock mode processes (SMP)

for ceria for maximum shock power. The ball to powder is ratio is 10:1. After every hour of milling, the mill is allowed to cool for 45 to 60 minutes. Toluene pre- vents excessive cold welding of the powder particles. The powders are milled for 20 hs and samples are col- lected regularly during milling to observe the progress of the size reduction. After attaining a reasonably small par- ticle size, the mill is stopped and the powder is washed with distilled water and then with ethyl alcohol followed by drying in air.

2.2. Liquid Processing—Solution Combustion Synthesis

Nanocrystalline cerium oxide particles are synthesized by a modified combustion process occurring from aque- ous solutions containing mixed fuels, *i.e.*, CAN with CA plus G. This type of mixed fuels has been already used by several researchers in the past [11,13]. The aqueous solution is prepared by dissolving the stoichiometric amount of ceric ammonium nitrate (CAN), $((NH_4)_2Ce(NO_3)_6)$ (Loba chemie, 99.5%) and glycine (G) and citric acid (CA) (Merck, 99.7%) in distilled water. The solution is then agitated in a beaker using magnetic stirrer for 3 h. The resulting solution is kept in an electric furnace set at 200°C. During the course of time, the solution evaporates, foams and then undergoes flameless combustion result- ing in nanocrystalline product. This fine powder is very light and porous.

Assuming complete combustion, the theoretical equa- tion for the formation of ceria can be written as follows:

$$CAN(aq) + (4/3)G(aq) + (2/3)CA(aq)$$
$$\rightarrow CeO_2(s) + (20/3)CO_2(g) + 10H_2O(g) + (14/3)N_2(g)$$
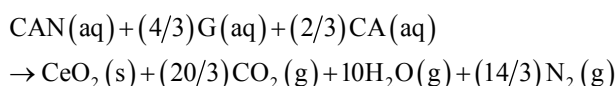
This as synthesised ceria powder is still impure as it contains the undissolved gases which are finally removed by calcinations at 500°C for 2 h in a muffle furnace.

3. Characterization

3.1. X-Ray Diffraction

All the samples have been characterized in a Phillips X-pert system diffractometer equipped with a Cu target operating at 40 kV and 40 mA that provides X-rays with $\lambda = 0.154$ nm. The particle size (d) and lattice strain (ε) are calculated by the most common Scherrer formula:

$$d = 0.9\lambda / B\cos\theta \qquad (1)$$

where, θ the Bragg angle and λ is the wavelength of the X-rays. The value of B in (1) is obtained from the re- lation $B^2 = B_S^2 - B_m^2$,
where B_S is the full width at half maximum intensity of the most prominent peak of the sample. The B_m, the instru- mental broadening, is the full width at half maximum

intensity of the corresponding peak from a strain free, coarse-grained sample.

However, there are contributions from both the lattice strain (B_{ls}) as well as the crystal size (B_{cs}) on peak broaden- ing, which can be refined as follows:

The peak broadening due to the lattice strain is pro- portional to $\tan(\theta)$ and that due to the particle size is in- versely proportional to $\cos(\theta)$

$$B_{cs} = 0.9\left(\frac{\lambda}{d\cos\theta}\right) \qquad (2)$$

$$B_{ls} = \varepsilon\tan(\theta) \qquad (3)$$

where ε is the r.m.s. strain. Hence, the total broadening is

$$B = 0.9\left(\frac{\lambda}{d\cos\theta}\right) + \varepsilon\tan(\theta) \qquad (4)$$

On rearranging the terms, we get

$$B\cos(\theta) = 0.9\left(\frac{\lambda}{d}\right) + \varepsilon\sin(\theta) \qquad (5)$$

For the measurement of crystallite size (d) and lattice strain (ε) from the above relation, the following peaks of the ceria (111), (200), (220), (311), (222) and (400) are selected. When $B\cos(\theta)$ is plotted against $\sin(\theta)$, for dif- ferent values of reflections, straight line is obtained with slope (ε) and intercept at $0.9\left(\frac{\lambda}{d}\right)$, from where the crystallite size (d) and lattice strain (ε) can be determined [14].

3.2. Particle Size Distribution

The ceria powder particles are analysed for their particle size by a particle size distribution analyzer (Microtrac-Zetatrac). The measurement technique is that of dynamic light scattering of colloidal particles in suspension. A colloidal suspension of the powder particles is made in Triton X-100 solution. The velocity distribution of the particles suspended is known as function of particle size. Light scattered from each particle is Doppler-shifted by particle motion (Brownian motion). The optical system sends the signal to a photodetector and further analysed by Microtrac® FLEX Windows Software, using proprie- tary algorithms, to provide the particle size distribution.

3.3. Electron Microscopy

The morphology of the coatings and distribution of nanoceria particles are analysed using scanning electron microscope (Carl Zeiss Supra EVO 60) in secondary electron mode.

A transmission electron microscope (Philips Technai 2 Twin G220S) operating at 200 kV is also used to charac- terize the ceria nanoparticles at higher resolution. The

samples are prepared by ultrasonication of already dispersed ceria powder in alcohol for 5 hours. The final solution is then poured over a carbon coated grid followed by drying in open atmosphere, and then stored at room temperature for characterization.

4. Results and Discussions

4.1. X-Ray Diffraction

Figures 1(a)-(c) shows the X-ray diffraction patterns of the nanocrystalline cerium oxide powder (a) ball milled for 0 to 20 hs, the inset shows the broadening of the (111) peak with milling time, (b) change in particle size with milling time for 20 hs and (c) X-ray pattern for solution combustion synthesized ceria powder. The average particle size and lattice strain of ceria powder are calculated from the X-ray diffraction patterns and are shown in **Table 1**.

It is noted that from **Table 1** that the particle size and lattice strain of ball milled ceria varies from 191 nm (0 h) to 32 nm (20 h). However, the lattice strain increases from 0.49×10^{-3} (0 h) to 1.14×10^{-3} (15 h) ball milled ceria and then it decreases to 1.06×10^{-3} with further milling at 20 hs due to cold welding of the powder particles. It has been reported already that the individual particles get rotated in a way to minimize the lattice strain [15], while for the ceria produced by the SCS method, the calculated particle size is 20 - 30 nm and lattice strain is $(0.191 - 0.392) \times 10^{-3}$.

4.2. Particle Size Distribution Analysis

From **Figure 2(a)** it is observed that the size distribution of the ball milled ceria powder particles follows uni modal distribution with particle size varying from 28 to 570 nm. The mean value of the particle size distribution lies round 90 nm.

While the ceria produced by SCS method possess bimodal particle size distribution (**Figure 2(b)**). The first group of particles varies from 60 to 85 nm with a mean value of 58 nm, and while the second group comprises of particles in range 500 - 800 nm with a mean value of 452
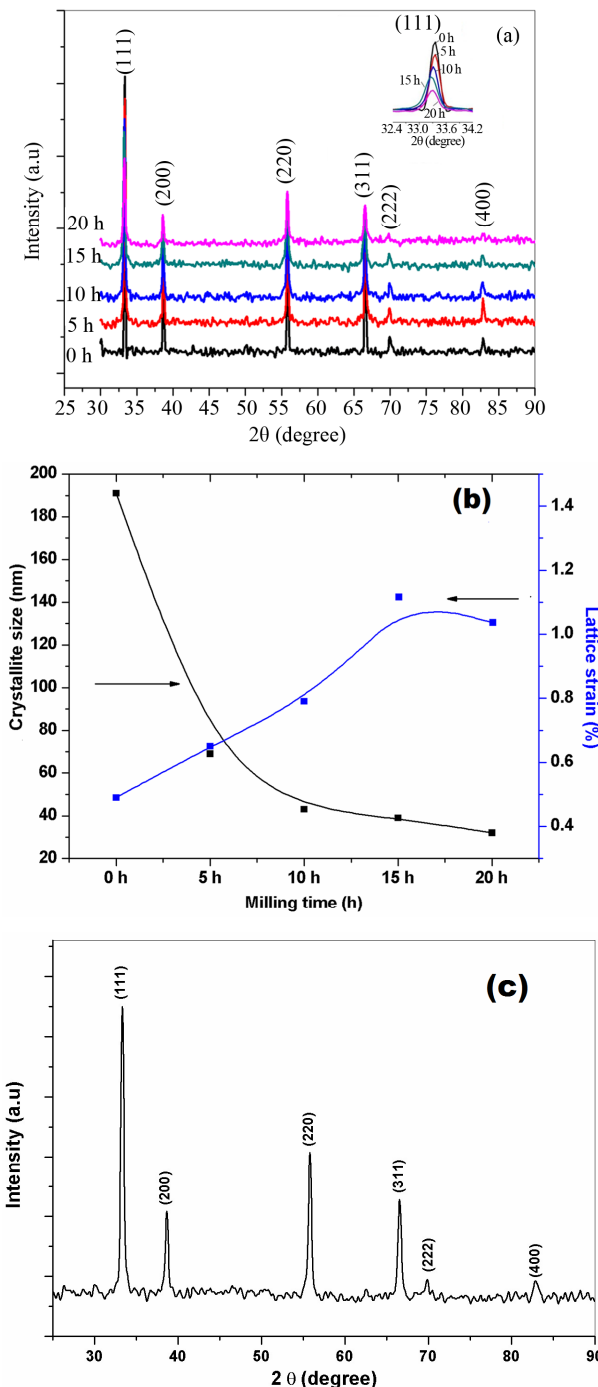

Figure 1. (a) X-ray diffraction patterns of (0, 5, 10, 15, and 20) hours ball milled ceria, (b) effect of milling time on particle size and lattice strain of ball milled ceria, and (c) X-ray diffraction pattern for solution combustion synthesized ceria.

nm. This indicates a greater tendency of ceria produced by SCS towards agglomeration. The degree of agglomeration in combustion synthesized ceria is well maintained at higher temperatures and is much higher as compared to that of ball milled ceria [16].

Table 1. Crystallite size and lattice strain.

Solid Route	HEBM	Crystallite Size (nm)	Lattice Microstrain (%)× 10⁻³
	0 h	191	0.49
	5 h	69	0.65
	10 h	43	0.79
	15 h	39	1.14
	20 h	32	1.06
Liquid Route	SCS	20 - 30	0.191 - 0.392

4.3. Electron Microscopy

4.3.1. SEM

It is observed from **Figures 3(a)-(b)** that the particle size of ceria is significantly reduced after ball milling and particle size is more or less uniform. The particles are faceted, free from porosity and irregular shaped in structure due to the continuous welding and fracturing and cold welding in due course of ball milling.

However, in case of ceria produced by SCS method, particles are present in the form of different sized lumps or flakes with rounded shaped structures, **Figure 3(c)**. This type of structures are generated due to the explosive nature of this reaction where gases evolve out giving rise to porosity, and thus the ceria produced by SCS shows a higher tendency towards agglomeration. The porous structure of the combustion synthesised powder was related with the structural rearrangement due to crystallization of the particles after calcinations [17].

4.3.2. TEM

From **Figure 4**, it is observed that ball milled ceria possess a range of particle size from 10 nm to 50 nm which are irregular shaped as show in **Figure 4(a)**. However, in case of combustion synthesized ceria the particle size is narrower, few particles are even approx. 10 nm (**Figure 4(b)**).

The ball milled ceria particles exhibits mixed formation of ring and spot diffraction pattern as shown in **Figure 4(c)**. In case of the ceria produced by SCS, the diffrac-
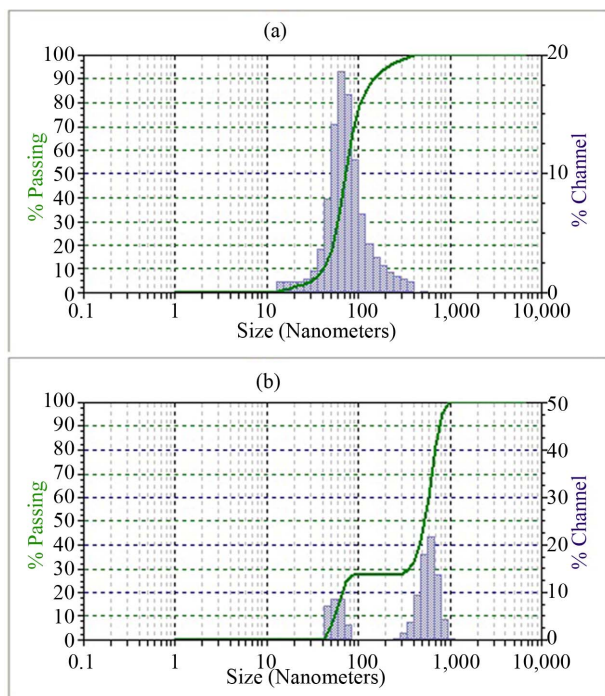
tion pattern consists of intense concentric rings, **Figure 4(d)**. These sharp rings are due to numerous single crystal diffraction from the randomly oriented crystals signifying
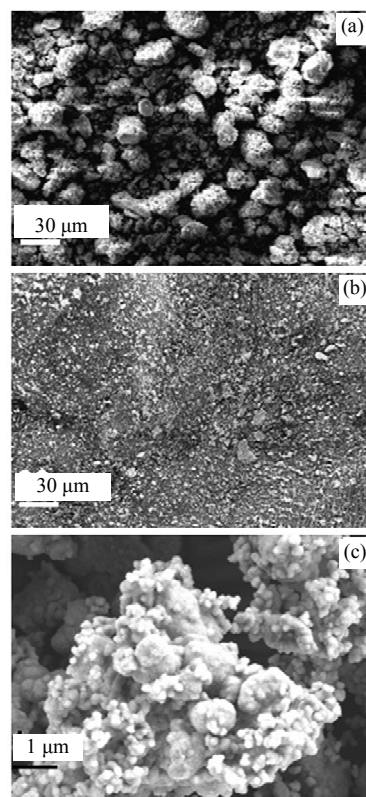

Figure 3. SEM micrograph of ceria powder prepared by ball milling (a) 0 h, (b) 20 h and (c) solution combustion synthesized ceria.
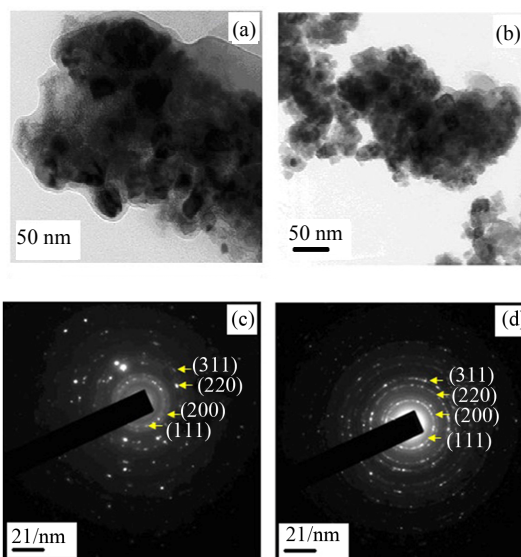

Figure 4. TEM micrographs of (a) 20 hs ball milled ceria powder and (b) combustion synthesized ceria powder; SAD patterns (c) 20 h ball ceria milled powder and (d) combustion synthesized ceria powder.

Figure 2. Particle size distribution of ceria (a) 20 h ball milled and (b) solution combustion synthesized ceria.

a finer crystallite sizes as compared to ball milled ceria powder particles.

5. Conclusions

1) The nanocrystalline ceria powder is successfully produced by both high energy ball milling and solution combustion synthesis methods.

2) The particle size distribution of ball milled ceria (28 - 570 nm) possesses a mean value of 90 nm as compared to that of combustion synthesized powder with a bimodal distribution (60 - 85 nm, and 500 - 800 nm) with mean values of 58 nm and 450 nm respectively.

3) There is significant porosity in solution combustion synthesized ceria as compared to that of ball milled ceria. The stability of porous structure of ceria produced by SCS at higher temperatures is the key to fabrication of new ordered and application in ceramic engineering. Thus, ceria produced by SCS route can be a better candidate for sensing applications.

REFERENCES

[1] H.-L. Chen, M.-H. Weng, S.-P. Ju, J.-G. Chang, H.-T. Chen and C.-S. Chang, "Structural and Electronic Properties of Ce_nO_{2n} ($n = 1 − 5$) Nanoparticles: A Computational Study," *Journal of Molecular Structure*, Vol. 963, No. 1, 2010, pp. 2-8.
doi:10.1016/j.molstruc.2009.09.019

[2] P. Knauth and H. L. Tuller, "Solute Segregation, Electrical Properties and Defect Thermodynamics of Nanocrystalline TiO_2 and CeO_2," *Solid State Ionics*, Vol. 136-137, 2000, pp. 1215-1224.
doi:10.1016/S0167-2738(00)00588-9

[3] Y. L. Xuan, J. Hu, K. L. Xu, X. D. Hou and Y. Lv, "Development of Sensitive Carbon Disulfide Sensor by Using Its Cataluminescence on Nanosized-CeO_2," *Sensors and Actuators B*, Vol. 136, 2009, pp. 218-223.
doi:10.1016/j.snb.2008.10.014

[4] G. I. N. Waterhouse and M. R. Waterland, "Opal and Inverse Opal Photonic Crystals: Fabrication and Characterization," *Polyhedron*, Vol. 26, 2007, pp. 356-368.
doi:10.1016/j.poly.2006.06.024

[5] Alan V. Chadwick and Shelley L.P. Savin, "EXAFS Study of Nanocrystalline CeO_2 Samples Prepared by Sol-Gel and Ball-Milling Routes," *Journal of Alloys and Compounds*, Vol. 488, 2009, pp. 1-4.
doi:10.1016/j.jallcom.2006.10.164

[6] H. S. Kang, Y. C. Kang, H. Y. Koo, S. H. Ju, D. Y. Kim, S. K. Hong, J. R. Sohn, K. Y. Jung and S. B. Park, "Nano-Sized Ceria Particles Prepared by Spray Pyrolysis Using Polymeric Precursor Solution," *Materials Science and Engineering B*, Vol. 127, No. 2-3, 2006, pp. 99-104.
doi:10.1016/j.mseb.2005.09.063

[7] A. Q. Wang, P. Punchaipetch, R. M. Wallace and T. D. Golden, "X-Ray Photoelectron Spectroscopy Study of Electrodeposited Nanostructured CeO_2 Films," *Journal of Vaccum Science Technology B*, Vol. 21, No. 3, 2003, p. 1169. doi:10.1116/1.1577569

[8] S. Kanakaraju, S. Mohan and A. K. Sood, "Optical and Structural Properties of Reactive Ion Beam Sputter Deposited CeO_2 Films," *Thin solid films*, Vol. 305, No. 1-2, 1997, pp. 191-195. doi:10.1016/S0040-6090(97)00081-3

[9] Y. Konishi, S. Asai, T. Murai and H. Takemori, "Preparation of Fine Ceria Powders by Cerium(IV) Carboxylate Solutions," *Metallurgical and Materials Transactions B*, Vol. 28, 1997, pp. 959-961.

[10] John J. Moore and H. J. Feng, "Combustion Synthesis of Advanced Materials: Part I. Reaction Parameters," *Progress in Materials Science*, Vol. 39, 1995, pp. 243-273.
doi:10.1016/0079-6425(94)00011-5

[11] R. D. Purohit, B. P. Sharma, K. T. Pillai and A. K. Tyagi, "Ultrafine Ceria Powders via Glycine-Nitrate Combustion," *Materials Research Bulletin*, Vol. 36, No. 15, 2001, pp. 2711-2721. doi:10.1016/S0025-5408(01)00762-0

[12] R. Hamzaoui, O. Elkedim and E. Gaffet, "Milling Conditions Effect on Structure and Magnetic Properties of Mechanically Alloyed Fe-10% Ni and Fe-20% Ni Alloys," *Materials Science and Engineering A*, Vol. 381, No. 1-2, 2004, pp. 363-371. doi:10.1016/j.msea.2004.05.008

[13] K. C. Patil, S. T. Aruna and T. Mimani, "Combustion Synthesis: An Update," *Current Opinion in Solid State and Materials Science*, Vol. 6, No. 6, 2002, pp. 507-512.
doi:10.1016/S1359-0286(02)00123-7

[14] C. Suryanarayana, "Mechanical Alloying and Milling," Marcell Dekker, New York, 2004.
doi:10.1201/9780203020647

[15] H. J. Fecht, Nanophasematerials-Syntheses, Properties and Applications: Proceedings of the NATO Advanced Study Institute on, Kluwer Academic Publishers, 1994, p. 125

[16] S. T. Mukherjee, V. Bedekar, A. Patra, P. U. Sastry and A. K. Tyagi, "Study of Agglomeration Behavior of Combustion-Synthesized Nano-Crystalline Ceria Using New Fuels," *Journal of Alloy and Compounds*, Vol. 466, No. 1-2, 2008, pp. 493-497.
doi:10.1016/j.jallcom.2007.11.070

[17] R. P. S. Chakradhar, B. M. Nagabhushana, G. T. Chandrappa, K. P. Ramesh and J. L. Rao, "Solution Combustion Synthesis Derived Nanocrystalline Macroporous Wollastonite Ceramics—Review," *Materials Chemistry and Physics*, Vol. 95, No. 1, 2006, pp. 169-175.
doi:10.1016/j.matchemphys.2005.06.002